Title
Object-Detecting Neurons in Drosophila

Journal
Current Biology, 27(5)

ISSN
0960-9822

Authors
Keleş, Mehmet F
Frye, Mark A

Publication Date
2017-03-01

DOI
10.1016/j.cub.2017.01.012

Peer reviewed

HHS Public Access

Author manuscript

Curr Biol. Author manuscript; available in PMC 2018 March 06.

Published in final edited form as:

Curr Biol. 2017 March 06; 27(5): 680–687. doi:10.1016/j.cub.2017.01.012.

Object detecting neurons in *Drosophila*

Mehmet F. Keleş[1] and **Mark A. Frye**[1,*]

[1]Department of Integrative Biology and Physiology, University of California - Los Angeles, Los Angeles, CA 90095

SUMMARY

Many animals rely on vision to detect objects such as conspecifics, predators, and prey. Hypercomplex cells found in feline cortex and small target motion detectors found in dragonfly and hoverfly optic lobes demonstrate robust tuning for small objects with weak or no response to larger objects or movement of the visual panorama [1–3]. However, the relationship between anatomical, molecular, and functional properties of object detection circuitry is not understood. Here, we characterize a specialized object detector in Drosophila, the lobula columnar neuron LC11 [4]. By imaging calcium dynamics with two-photon excitation microscopy we show that LC11 responds to the omni-directional movement of a small object darker than the background, with little or no responses to static flicker, vertically elongated bars, or panoramic gratings. LC11 dendrites innervate multiple layers of the lobula, and each dendrite spans enough columns to sample 75-degrees of visual space, yet the area that evokes calcium responses is only 20-degrees wide, and shows robust responses to a 2.2-degree object spanning less than half of one facet of the compound eye. The dendrites of neighboring LC11s encode object motion retinotopically, but the axon terminals fuse into a glomerular structure in the central brain where retinotopy is lost. Blocking inhibitory ionic currents abolishes small object sensitivity and facilitates responses to elongated bars and gratings. Our results reveal high acuity object motion detection in the *Drosophila* optic lobe.

RESULTS AND DISCUSSION

Whether flying or walking, flies readily orient toward large moving objects such as elongated vertical bars or edges representing landscape features, and this behavior is mediated by interactions between motion vision and motion-independent feature detection [5–8]. Flies are able to perform some object-directed behaviors when directionally selective columnar motion detectors (T4 and T5) supplying the third optic ganglion (lobula plate) are silenced [6,7,9]. This finding supports the existence of object detection circuitry that acts independently from the canonical motion vision pathway [6]. Whereas many of the cells,

*Correspondence, lead contact: frye@ucla.edu.

Author Contributions: M.F.K. and M.A.F. designed the research and wrote the manuscript. M.F.K. conducted the experiments and analyzed the data.

circuits and computations for motion processing by T4 and T5 and the downstream lobula plate are becoming ever clearer [10–13], the circuitry and functional role of the neighboring neuropile, the lobula, which houses 80% of all neurons in the lobula complex [14], is poorly understood in *Drosophila*.

The lobula contains more than 22 types of visual projection neurons (VPNs) including lobula columnar (LC) neurons that project to the ventrolateral protocerebrum (VLPR) and form synapse-rich output domains called optic glomeruli for their structural similarity to olfactory glomeruli [4,15,16]. Neurons downstream of LCs that interconnect multiple optic glomeruli in the central brain respond to small objects [17], raising the possibility that select LCs may themselves be tuned to small objects. Optophysiological and electrophysiological methods have demonstrated that several LCs are broadly sensitive to visual features such as edges or bars [18,19], yet no study to date has thoroughly explored LCs with small two-dimensional objects.

We visually screened the publicly-available Janelia Gal4 lines [20] and identified the R22H02-Gal4 driver which labels ~51 LC11s (±4, n=5) and each LC11 neuron has dendritic arborizations in layers 2,3,4 and 5 of the lobula (Figure 1A–C Figure S1A and C, [16]). The dendrites of a single LC11 span 14–15 lobula columns in the dorso-ventral axis and 6–8 columns in the antero-posterior axis (Figure 1 C and D). Taking into account that LC11 dendrites form an ellipse in the lobula (Figure 1E), we estimated the total span of a single LC11 to be 65 to 85 neighboring columns thereby comprising a ‘multi-pixel’ neuron. Considering the dendritic span (~15×8 columns), the number of LC11 cells (~50), and the full array of retinal ommatidia and neuopile columns (~28×28), it would seem that LC11 dendrites must overlap with one another rather extensively. Multicolor stochastic labeling of individual cells confirmed that LC11s overlap rather than tile the lobula (Figure 1F–I). Sampling the inputs of many columns could underlie spatial pooling important for increased photon capture in dim light [21].

Previous work suggested that all LC11 output synapses are confined to the cognate glomerulus within the posterior VLP (PVLP) [4,15]. We observe presynaptic sites not only in the PVLP glomerulus but also within layer 5 innervations of LC11 (Figure S1A and S1B), consistent with other recent findings by a recent article [16]. A second distinct cell labeled by our Gal4 line is intrinsic to the lobula near the base of LC11 dendrites (Figure S1C, and Supplemental Experimental Procedures). Calcium imaging from dendrites could have been contaminated by the intrinsic cell, but this seems unlikely since dendritic responses were consistently identical to cell body and axon terminal responses in LC11 (see below).

By contrast to the retinotopic organization of the columnar dendrites in the lobula, labeling a single LC11 neuron reveals spatially-distributed presynaptic terminals ramifying throughout the output glomerulus formed by LC11 terminals (Figure 1Bi–ii). Furthermore, multicolor labeling of two individual LC11 cells (Figure S1D) shows fully interspersed axon terminals (Figures S1E,F). This convergent organization indicates the loss of retinotopic structure by LC11 within the glomerulus, consistent with findings in other LCs [15,16].

To physiologically characterize LC11, we utilized GCaMP6m under two-photon imaging (Figure 1J,K) to record LC11 dendrites, axon terminals, and cell bodies (see Figure S1G–I for ROI images) in response to an object that may represent another fly nearby or a larger animal moving at a distance, a vertical bar that may represent a landscape feature such as a plant stalk, and a rotating wide-field grating representing optic flow generated during self-motion. We recorded from the axon terminals of LC11 (Figure S1I) and observed large responses to a 30 by 8 degree object (Figure 1L). The response diminished markedly for the vertical bar, and there was no response to the wide-field grating (Figure 1L). We tested whether LC11 is necessary for avoidance of similarly sized objects in flight [22], but did not observe a clear phenotype (Figure S1J–L). LC11 could instead contribute to social behaviors such as courtship [9,23]. Alternatively, given the complex spatial interactions of LC11 and its normal mode of action by individual members of the columnar array, activating or inactivating the entire population may produce spurious effects within the visual system.

Drosophila can detect and respond to objects that appear smaller than 5° [24]. We found that a moving 2.2° object drove LC11 responses well above noise and greater than half-amplitude response to a 4.4° object (Figure 1M). Both objects span less than one inter-ommatidial separation angle of 5° [25]. To confirm that flies are capable of perceiving such small objects on our LED display, we used a systems identification method during tethered flight [26] to show robust steering responses to either a single pixel object or two-pixel object displaced in single-pixel increments (Figure 1M inset). In principle, any photoreceptor could respond to the luminance decrement generated by an object spanning less than its total acceptance angle, yet it is remarkable that simple hyperacuity has been documented within lobula neurons of hoverflies [3] and more recently within *Drosophila* photoreceptors [27].

We next compared the calcium response dynamics within dendrites, cell bodies, and axon terminals in the same preparation. Normalized response trajectories demonstrated that dendrite and terminal responses were temporally synchronized (Figure 1N), but by comparison cell bodies exhibited a significantly delayed response onset (Figure 1O) followed by a slow decay to baseline. These differences may be attributed to the unipolar morphology of some invertebrate neurons such as LC11, in which the cell body is situated at the end of a long neurite and does not participate in synaptic integration.

Despite the slow response kinetics, imaging from the cell bodies is required to access individual neurons within the palisade of labeled LC11 cells due to the spatial intermingling of their dendrites and axon terminals (Figure S1D–F). To map the receptive field of individual LC11s we swept an 8.8° square object in horizontal and vertical directions at each elevation and azimuthal angle, respectively (Figure 2A). For each LC11 recording, peak ΔF/F values were fit to Gaussian functions of azimuth and elevation and used to estimate the two-dimensional spatial receptive field (Figure 2B and S2). We enclosed the spatial receptive field with a contour representing the full-width at 25% max of the Gaussian fits (Figure 2B, see Supplemental Experimental Procedures). We were generally able to record several distinct LC11 cell bodies from each preparation (Figure 2C). Some receptive fields we sampled overlapped, providing functional evidence that individual LC11s have overlapping dendrites (Figure 2C). Although we did not record from all LC11s, the receptive

fields of those we sampled were distributed throughout the frontolateral visual field (Figure 2D and D′). The average receptive field size was 24.1° by 18.8° with standard deviation of 5.7° and 5.7°, respectively, measured from 27 individual cell recordings. The functional receptive field size is well below the anatomical dendritic field size (70°–75° by 30°–40°, Figure 1), a property unique to LC11 by comparison to neurons of the lamina, medulla or lobula plate identified to date [28–30].

To confirm whether or not the population of LC11 dendrites samples the full visual field in a retinotopic manner, we imaged from dendritic arborizations of many LC11s simultaneously and scanned an object horizontally at varying elevation angles (Figure 2E). Objects that are presented at higher elevations elicited responses from anteriorly located dendrites (Figure 2E′). Shifting the object from higher to lower elevations on the display corresponded to shifts in calcium responses from anterior to posterior dendrites (Figure 2E′) confirming the retinotopic organization of LC11 dendritic inputs and suggesting that the visual field is sampled uniformly.

Given the sluggish on and off response kinetics observed in the cell bodies (Figure 1N), the tight temporal coupling between GCaMP responses in the dendrites and axon terminals (Figure 1N), and the innervation by individual LC11 cells throughout the output glomerulus (Figure 1Bi–ii, Figure S1E and F), we characterized the object response properties of LC11 with recordings from the axon terminals in the VLPR. Small target motion detectors (STMDs) examined to date in the dragonfly [31] and hoverfly [3] show preference for objects darker than the background. We therefore presented a light object moving across a dark background (ON) and dark object moving on a light background (OFF) (Figure 3A). Our results indicate that LC11 responds to both OFF and ON stimuli to varying extent, showing significant preference for OFF (Figure 3A′, paired t-test $p<0.001$). Another characteristic feature of STMDs is flicker insensitivity [32]. Stimulating luminance increments (ON) or decrements (OFF) by a stationary object localized within the receptive failed to elicit responses in LC11 terminals (Figure 3A″).

We next systematically varied the brightness of an object moving across a fixed intensity background (Figure 3B). Interestingly, reduction of the OFF-object contrast from 100% to 30% nearly doubled the amplitude of the calcium response (Figure 3B′). The object size in these experiments (30°) was chosen based on prior behavioral findings [22], yet is larger than the estimated receptive field size (24°). It is likely that a 30° object traverses both the excitatory receptive field and the inhibitory end zones. Reducing the contrast of a sufficiently large object may in turn reduce the inhibition generated by the object edges, resulting in increased response amplitude observed in LC11 for reduced contrast (Figure 3B′). LC11 responds only weakly to moving ON objects and does not show a significant change in amplitude across contrast (Figure 3B′), providing more evidence that LC11 is OFF object-specific. In flies, ON and OFF signals are separated within the lamina and relayed to deeper neuropils via parallel pathways [10,12,13,33,34]. Layers 2–4 of lobula are innervated by ON-selective Tm3 and OFF-selective Tm4 neurons [16,35]. LC11 could potentially receive direct input from parallel ON and OFF channels *via* Tm3 and Tm4. Correlating a delayed OFF signal with an un-delayed ON signal arising from a single photoreceptor, i.e. within the same column, fully captured the contrast selectivity of the

dragonfly STMD [31] and suggests a potential mechanism for small object sensitivity by LC11.

We next tested for directional selectivity by moving an 8.8° by 8.8° object in eight different directions. The recordings show that LC11 is not significantly selective for motion direction (Figure 3C and C′, one-way ANOVA n.s.), although shows a slight trend for vertical directions, which is consistent with previous membrane patch clamp recordings from the soma [19]. The glomerular output from the population of LC11s therefore serves to detect an object moving in any direction through the receptive field, a finding which we corroborated at the level of individual LC11s (Figure S3B and S3B′).

The selectivity for small moving objects over elongated bars suggests that LC11 is size-tuned. The classical mechanism for size tuning is end-stopped inhibition, a hypercomplex property in which an elongated contour stimulates the inhibitory end zones of a receptive field with an excitatory center [1]. We parameterized the vertical dimension of a horizontally moving object of fixed width. Note that most of our experiments move an object in the horizontal (azimuthal) direction, and thus the characteristic object size is defined as the angle subtended by the vertical edge, perpendicular to the axis of movement. The optimum LC11 response occurs for a vertical extent of 8.8°, which is $1/4^{th}$ the vertical projection of the anatomical receptive field or ½ the functional receptive field (Figure 3D). The response magnitude asymptotes as the vertical size spans one functional receptive field (Figure 3D′).

To test whether LC11 is size-tuned in the dimension parallel with the axis of motion, we presented objects of fixed vertical height and varying horizontal widths moving horizontally. For objects of increasing width, the response amplitude peaked near 4.4° (Figure 3E). The peak amplitude decreased until the width of the object was approximately one LC11 receptive (24°) (Figure 3E′). Note that the vertically oriented object moving horizontally generates more inhibition (Figure 3D, responses are clipped for the largest vertical bar) than an object oriented horizontally moving parallel to its orientation (Figure 3E, half-maximum response remain for largest horizontal bar). This would be expected because the former object stimulates more ommatidia, thus activates more LC receptive fields and their presynaptic inputs, and thereby generates more spatial inhibition. Furthermore, parameterizing the vertical size of the horizontally moving object (Figure 3D), we would expect each object to sweep through different numbers of LC11 receptive fields in time, resulting in varying onset timing of the GCaMP signals in the glomerulus for each size (Figure 3D). By contrast, for the horizontally moving object, the spatial extent of the stimulus orthogonal to the motion vector is invariant and therefore the leading edge stimulates the same ensemble of LC11 receptive fields for each stimulus size. Hence, the onset delay is invariant for this experiment (Figure 3E).

Owing to the close match between the spatial extent of the receptive field and optimum object size, we reasoned that the end-stopped property of LC11 could be shaped by lateral inhibition generated by nearest neighbor LC11s. If so, then the end-stopped inhibition generated by two nearby objects should be fully relieved once the objects are separated by one receptive field increment. By presenting two 8.8° square objects moving horizontally, we confirmed that as spatial inhibition was released by increased object separation, response

amplitude increased (Figure 3F). The separation distance had no effect on response amplitude once the two objects were separated by 18°, roughly the size of a single LC11's functional receptive field (Figure 3F′). Furthermore, separation distances flanking the preferred object size (8.8°) led to the biggest change in response amplitude. These results support the hypothesis that end-stopped inhibition occurs on the spatial scale of nearest neighbor LC11 functional receptive fields.

One consistent characteristic of the response to two objects is a 'double peak' for object separation less than 18° (Figure 3E). We did not observe this bi-phasic response when presenting the same stimuli in the reverse back-to-front direction (Figure S3A and A′). Thus, we attribute the 'double peak' phenomenon either to subtle differences in the spatial distribution of LC11 receptive fields converging in the axon terminals, or to differences in the spatial properties of inhibition between the lateral-ventral field of view by comparison to the frontal-dorsal field.

Taken together, the results presented thus far implicate end-stop lateral inhibition in sculpting object response properties, suggesting that LC11 may receive GABAergic input. Previous immunohistochemical studies of the lobula indicate that antibodies targeting GABAergic signaling pathways such as glutamic acid decarboxylase (GAD), the $GABA_A$ receptor subunit RDL, and GABA itself, are present in a layer-specific manner [36,37]. In particular, an enrichment of GABAergic neurotransmission, indicated by dense labeling of all three antibodies, is observed in layers 2 and 3 of the lobula. Our own co-labeling experiments indicate a strong overlap between the dendritic arborizations of LC11 and enriched vesicular GABA transporter (VGAT) staining (Figure 4A and C). In contrast, the dendrites of LC11 are spatially-excluded from layer 1, known to be enriched with cholinergic signaling within T5 cells (Figure 4B and D) [38].

To test for functional consequences of GABAergic inhibition on the response properties of LC11, we imaged from the LC11 glomerular outputs before and after blocking $GABA_A$-mediated inhibitory currents with picrotoxin (PTX). Prior to PTX application, LC11 responded robustly to an object, showed a slight excitation in response to a bar, and was not at all excited by a wide-field grating (Figure 4E,F and G). Applying PTX in the perfusion saline within the same recording preparations resulted in strongly reduced object responses, large amplitude bar responses, and large amplitude sustained responses to wide-field motion (Figure 4E,F, and G). Remarkably, PTX not only resulted in a loss of selectivity for an object, but also small sensitivity to the object (Figure 4E′, F′ and G′). Thus, inhibitory currents not only 'end-stop' LC11 to tune its size selectivity, similar currents also actively mediate the detection of small objects. By contrast, figure detecting cells (FD) of the lobula plate in larger flies are excited by small-field gratings and receive GABAergic inhibition from wide-field cells, yet under GABA-blockade FD continues to respond to small-field motion [39]. In STMDs, small object tuning has been attributed to lateral inhibition at the level of pre-synaptic neighboring ON-OFF channels that are correlated and summed [31,40]. However, in the absence of inhibition the model described in [31,40] predicts that STMDs would be driven by dark edges of any size. Our finding that small object detection itself requires intact inhibition (Figure 4E) may come to promote a revised model.

The finding that LC11 dendrites span 14–15 columns of the optic lobe yet the functional receptive field is the equivalent of 4–6 columns wide, with peak size tuning less than the equivalent of two columns, suggests complex inhibitory spatial interactions. We propose that an excitatory-center inhibitory-surround mechanism, driven by inhibition on the spatial scale of a neighboring LC11, spatially sharpens the receptive field of LC11 making it both sensitive and selective for small contrasting objects. In summary, we show the first comprehensive physiological characterization of object selectivity by a visual projection neuron in *Drosophila*, one that shares functional properties of object detectors in other insects and vertebrates.

Supplementary Material

Refer to Web version on PubMed Central for supplementary material.

Acknowledgments

We thank Jaison Omoto for carefully reading the manuscript, Jacob Aptekar for experimental help and contribution to the subpanel of Figure 1M, Volker Hartenstein for confocal microscope use and Frye lab members for helpful discussion, Aljoscha Nern and Michael Reiser for lobula layer identification and kindly discussing unpublished results, David Krantz for the VGAT antibody. This research was supported by the UCLA Edith Hyde Fellowship (M.F.K.), and National Institutes of Health EY026031 (M.A.F.).

References

1. Hubel DH, Wiesel TN. Receptive fields, binocular interaction and functional architecture in the cat's visual cortex. J Physiol. 1962; 160:106–154.2. [PubMed: 14449617]
2. O'Carroll D. Feature-detecting neurons in dragonflies. Nature. 1993; 362:541–543.
3. Nordström K, O'Carroll DC. Small object detection neurons in female hoverflies. Proc Biol Sci. 2006; 273:1211–1216. [PubMed: 16720393]
4. Otsuna H, Ito K. Systematic analysis of the visual projection neurons of Drosophila melanograster. I. Lobula-specific pathways. J Comp Neurol. 2006; 497:928–958. [PubMed: 16802334]
5. Aptekar JW, Shoemaker PA, Frye MA. Figure tracking by flies is supported by parallel visual streams. Curr Biol. 2012; 22:482–487. [PubMed: 22386313]
6. Bahl A, Ammer G, Schilling T, Borst A. Object tracking in motion-blind flies. Nat Neurosci. 2013; 16:730–8. [PubMed: 23624513]
7. Bahl A, Serbe E, Meier M, Ammer G, Borst A. Neural Mechanisms for Drosophila Contrast Vision. Neuron. 2015; 88:1240–1252. [PubMed: 26673659]
8. Poggio T, Reichardt W. Visual control of orientation behaviour in the fly: Part II. Towards the underlying neural interactions. Q Rev Biophys. 1976; 9:377. [PubMed: 790442]
9. Coen P, Xie M, Clemens J, Murthy M. Sensorimotor Transformations Underlying Variability in Song Intensity during Drosophila Courtship. Neuron. 2016; 89:629–644. [PubMed: 26844835]
10. Meier M, Serbe E, Maisak MS, Haag J, Dickson BJ, Borst A. Neural circuit components of the Drosophila OFF motion vision pathway. Curr Biol. 2014; 24:385–392. [PubMed: 24508173]
11. Maisak MS, Haag J, Ammer G, Serbe E, Meier M, Leonhardt A, Schilling T, Bahl A, Rubin GM, Nern A, et al. A directional tuning map of Drosophila elementary motion detectors. Nature. 2013; 500:212–6. [PubMed: 23925246]
12. Ammer G, Leonhardt A, Bahl A, Dickson BJJ, Borst A. Functional Specialization of Neural Input Elements to the Drosophila on Motion Detector. Curr Biol. 2015; 25:2247–2253. [PubMed: 26234212]
13. Joesch M, Schnell B, Raghu SV, Reiff DF, Borst A. ON and OFF pathways in *Drosophila* motion vision. Nature. 2010; 468:300–4. [PubMed: 21068841]
14. Strausfeld, NJ. Atlas of an Insect Brain. Vol. 52. Springer; 1976. p. 1096-1109.

15. Panser K, Tirian L, Schulze F, Villalba S, Jefferis GSXE, Bühler K, Straw AD. Automatic Segmentation of Drosophila Neural Compartments Using GAL4 Expression Data Reveals Novel Visual Pathways. Curr Biol. 2016; 26:1943–1954. [PubMed: 27426516]
16. Wu M, Nern A, Williamson WR, Morimoto MM, Reiser MB, Card GM, Rubin GM. Visual projection neurons in the Drosophila lobula link feature detection to distinct behavioral programs. Elife. 2016; 5
17. Kim AJ, Fitzgerald JK, Maimon G. Cellular evidence for efference copy in Drosophila visuomotor processing. Nat Neurosci. 2015; 18:1247–1255. [PubMed: 26237362]
18. Aptekar JW, Keleş MF, Lu PM, Zolotova NM, Frye MA. Neurons forming optic glomeruli compute figure-ground discriminations in Drosophila. J Neurosci. 2015; 35:7587–99. [PubMed: 25972183]
19. Mu L, Ito K, Bacon JP, Strausfeld NJ. Optic Glomeruli and Their Inputs in Drosophila Share an Organizational Ground Pattern with the Antennal Lobes. J Neurosci. 2012; 32:6061–6071. [PubMed: 22553013]
20. Jenett A, Rubin GM, Ngo TTB, Shepherd D, Murphy C, Dionne H, Pfeiffer BD, Cavallaro A, Hall D, Jeter J, et al. A GAL4-Driver Line Resource for Drosophila Neurobiology. Cell Rep. 2012; 2:991–1001. [PubMed: 23063364]
21. Warrant EJ, Kelber A, Gislén A, Greiner B, Ribi W, Wcislo WT, von Frisch K, Cartwright BA, Collett TS, Rossel S, et al. Nocturnal vision and landmark orientation in a tropical halictid bee. Curr Biol. 2004; 14:1309–18. [PubMed: 15296747]
22. Maimon G, Straw AD, Dickinson MH. A Simple Vision-Based Algorithm for Decision Making in Flying Drosophila. Curr Biol. 2008; 18:464–470. [PubMed: 18342508]
23. Agrawal S, Safarik S, Dickinson M. The relative roles of vision and chemosensation in mate recognition of Drosophila melanogaster. J Exp Biol. 2014; 217:2796–805. [PubMed: 24902744]
24. Zabala F, Polidoro P, Robie A, Branson K, Perona P, Dickinson MH. A simple strategy for detecting moving objects during locomotion revealed by animal-robot interactions. Curr Biol. 2012; 22:1344–1350. [PubMed: 22727703]
25. Heisenberg, M., Wolf, R. Vision in Drosophila, genetics of microbehavior. New York: Springer-Verlag; 1984.
26. Theobald JC, Ringach DL, Frye MA. Dynamics of optomotor responses in Drosophila to perturbations in optic flow. J Exp Biol. 2010; 213:1366–75. [PubMed: 20348349]
27. Juusola M, Dau A, Song Z, Solanki N, Rien D, Jaciuch D, Dongre S, Blanchard F, de Polavieja GG, Hardie RC, et al. Microsaccadic information sampling provides Drosophila hyperacute vision. bioRxiv. 2016
28. Behnia R, Clark DA, Carter AG, Clandinin TR, Desplan C. Processing properties of ON and OFF pathways for Drosophila motion detection. Nature. 2014; 512:427–430. [PubMed: 25043016]
29. Tuthill JC, Nern A, Rubin GM, Reiser MB. Wide-Field Feedback Neurons Dynamically Tune Early Visual Processing. Neuron. 2014; 82:887–895. [PubMed: 24853944]
30. Schnell B, Joesch M, Forstner F, Raghu SV, Otsuna H, Ito K, Borst A, Reiff DF. Processing of horizontal optic flow in three visual interneurons of the Drosophila brain. J Neurophysiol. 2010; 103:1646–1657. [PubMed: 20089816]
31. Wiederman SD, Shoemaker PA, O'Carroll DC. Correlation between OFF and ON channels underlies dark target selectivity in an insect visual system. J Neurosci. 2013; 33:13225–32. [PubMed: 23926274]
32. Barnett PD, Nordström K, O'Carroll DC. Retinotopic Organization of Small-Field-Target-Detecting Neurons in the Insect Visual System. Curr Biol. 2007; 17:569–578. [PubMed: 17363248]
33. Serbe E, Meier M, Leonhardt A, Borst A. Comprehensive Characterization of the Major Presynaptic Elements to the Drosophila OFF Motion Detector. Neuron. 2016; 89:829–841. [PubMed: 26853306]
34. Strother JA, Nern A, Reiser MB. Direct observation of on and off pathways in the drosophila visual system. Curr Biol. 2014; 24:976–983. [PubMed: 24704075]
35. Fischbach KF, Dittrich AP. The optic lobe of Drosophila melanogaster. I: A Golgi analysis of wild-type structure. Cell Tissue Res. 1989; 258:441–475.

36. Buchner E, Bader R, Buchner S, Cox J, Emson PC, Flory E, Heizmann CW, Hemm S, Hofbauer A, Oertel WH. Cell-specific immuno-probes for the brain of normal and mutant Drosophila melanogaster - I. Wildtype visual system. Cell Tissue Res. 1988; 253:357–370. [PubMed: 2900684]

37. Harrison JB, Chen HH, Sattelle E, Barker PJ, Huskisson NS, Rauh JJ, Bai D, Sattelle DB. Immunocytochemical mapping of a C-terminus anti-peptide antibody to the GABA receptor subunit, RDL in the nervous system of Drosophila melanogaster. Cell Tissue Res. 1996; 284:269–278. [PubMed: 8625394]

38. Mauss AS, Meier M, Serbe E, Borst A. Optogenetic and pharmacologic dissection of feedforward inhibition in Drosophila motion vision. J Neurosci. 2014; 34:2254–63. [PubMed: 24501364]

39. Warzecha AK, Egelhaaf M, Borst A. Neural circuit tuning fly visual interneurons to motion of small objects. I. Dissection of the circuit by pharmacological and photoinactivation techniques. J Neurophysiol. 1993; 69:329–339. [PubMed: 8459270]

40. Wiederman SD, Shoemaker PA, O'Carroll DC. A model for the detection of moving targets in visual clutter inspired by insect physiology. PLoS One. 2008; 3

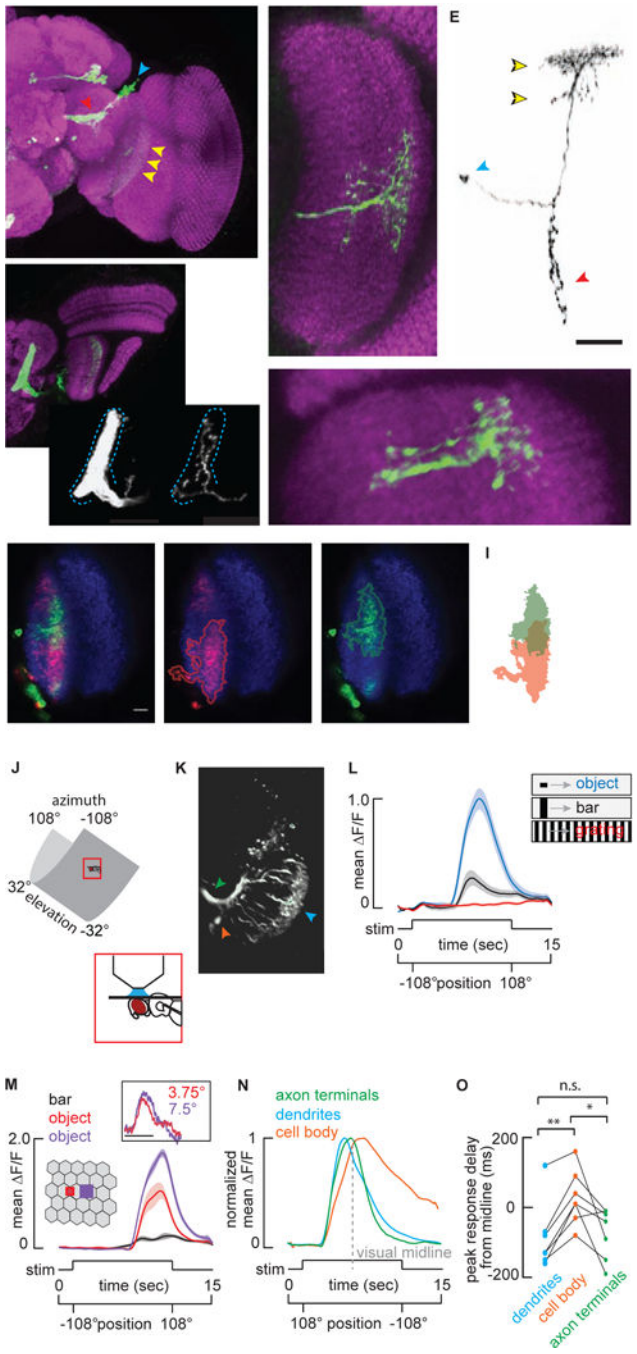

Figure 1. Anatomy and object selectivity of Lobula Columnar 11

A) Maximum intensity projection of the anterior view of a brain from a fly expressing membrane tethered GFP under the control of R22H02-Gal4 and labeled with anti-GFP (green) and nc82 (magenta). Dashed lines indicate the boundary of the ventrolateral protocerebrum. Arrowheads indicate cellular compartments; blue-cell bodies, red-terminals, yellow-dendrites. B) Dorsally mounted view of R22H02-Gal4>UAS-mCD8::GFP flies. Dashed rectangle indicates the unique foot shaped LC11 glomerulus. Me: Medulla, Lo: Lobula, LoP: Lobula Plate. Comparison of the labeling of ~50 LC11s innervating the

glomerulus (Bi) vs. stochastic labeling of a single LC11 (Bii). Single LC11 shows the full glomerular innervation with no evidence of retinotopic organization. Blue dashed line indicates the glomerular boundary. C) Anterior view of a stochastic labeling of a single LC11. Dashed lines indicate individual columns within the lobula. The dendritic arbor of a single LC11 covers about 14–15 lobula retinotopic columns in this plane. D) Dorsal view of a single LC11. Dendritic arbors span 6–7 columns in this plane. E) Morphology of a single LC11. Yellow arrows indicate the bistratified dendritic morphology of LC11 within lobula. Blue and red arrowheads indicate cell body and terminals respectively. All scale bars are 25 um. F–H) Single confocal plane images of multicolor stochastic labeling of LC11s. Multiple cells were labeled and tagged with myristoylated smGFP attached to either HA (green) or FLAG (red) epitopes. Neuropile is labeled with nc82 (blue). The lobula is traced with a dashed line. Scale bar is 10 um. G,H) Red and green channels are displayed separately, and labeling is traced to highlight dendritic overlap (I). See also Figure S1. J–O) 2-photon imaging. J) The fly's head is fixed and the surrounding LED arena covers 216° in azimuth and 63.2° in elevation. K) Image of LC11s expressing GCaMP6m under two-photon microscopy. Arrowheads indicate dendrites (cyan), axon terminals forming optic glomerulus (green) and cell bodies (orange). L) Mean GCaMP6m (±S.E.M. shading) signal from LC11 glomerulus in response to the movement of a 30°by 8.8° object (blue), a 30° by 70° bar (black) and a wide-field grating (red, n = 7 flies). M) Mean GCaMP6m (±S.E.M. shading) signal from LC11 glomerulus in response to the movement of a 30° by 70° bar (black), a 2.2° square object (red) and a 4.4° square object (purple) (n = 6 flies). Inset: From tethered flies, normalized mean steering responses to single pixel impulsive displacement of objects, sizes indicated (scale bar: t=0–100 ms, n = 10 flies). N) Normalized mean ΔF/F of cell body (orange), dendrites (cyan) and axon terminals (green) responses to the movement of a 30° by 8.8° object as in C. Visual midline indicated with a dashed grey line. n = 7 flies. O) Comparison of the peak onset delay between the dendrites (blue), terminal (red), and cell body (black) (*$p<0.05$, **$p<0.01$, paired t-test, n = 7 flies). All visual stimuli moved at 22 °/sec.

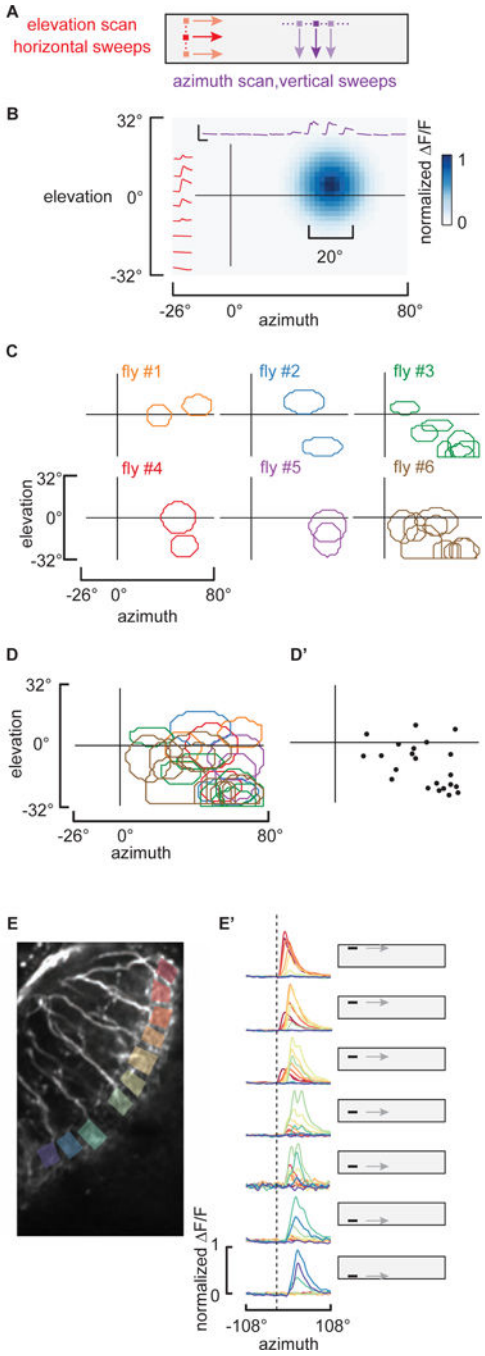

Figure 2. Individual LC11 receptive fields

A) Schematic of the experimental stimuli used to map individual LC11 receptive fields from individual cell body recordings. An 8.8° square dark object was scanned along non-overlapping trajectories along both horizontal and vertical paths at 33 °/sec. B) Reconstructed receptive field of a single LC11. Individual imaging responses from a single LC11 to the horizontal and vertical sweeps indicated in red and purple, respectively (scale bar inset represents 200% ΔF/F, 5 seconds). Reconstructed estimate of a single LC11 receptive field shown in blue (see Supplemental Experimental Procedures), the full-width at

25% max contour was drawn in white. C) Representative receptive field contours (25% max) from six preparations are mapped onto the projection of the visual display. D) 11 receptive fields from 6 flies are overlaid and color coded as in C. D′) a dot is plotted at the centroid of each receptive field to indicate the spatial distribution of sampled LC11 recordings. E) To analyze the retinotopy in the dendrites of neighboring LC11 columnar cells, ROIs from separate dendritic compartments are indicated by colored box. An object swept was horizontally at elevations indicated by the cartoon display. ΔF/F responses from all 10 ROIs are overlaid for each elevation. E′) To facilitate spatial comparisons, the responses are normalized to the maximum ΔF/F calcium signal at each ROI. Note that anterior (red) ROIs are activated by object motion across the top of the display, whereas posterior (blue) ROIs are activated by object motion across the bottom of the display. Dashed line indicates the earliest responses of anterior ROIs. Scale bar for the two-photon image represents 10 um. Abbreviations for anatomical directions; A: Anterior, P: Posterior, M: Medial and L: Lateral. See also Figure S2.

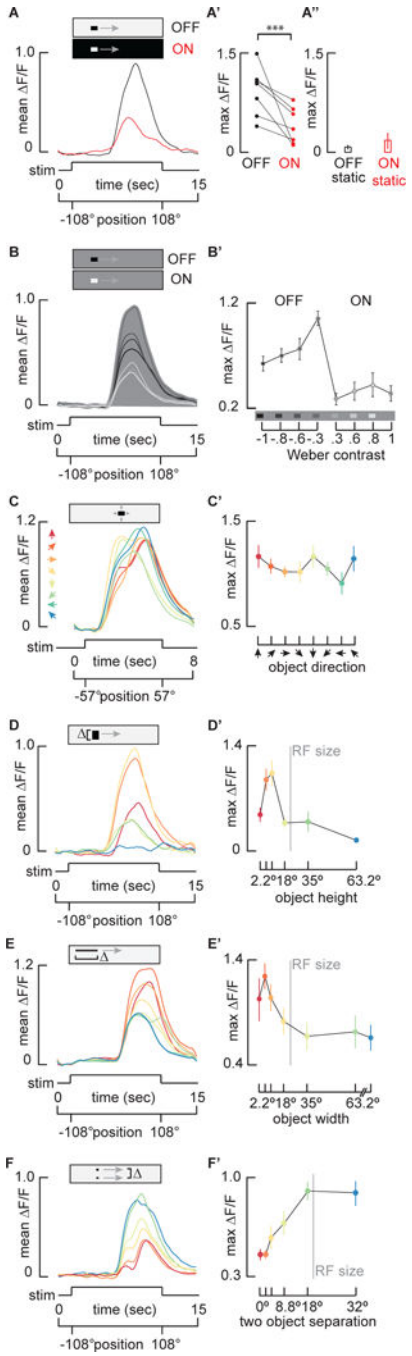

Figure 3. LC11 is contrast selective, omni-directional, and end-stopped on the spatial scale of one receptive field

A) Mean GCaMP6m signal from the LC11 terminal output glomerulus in response to a 30°by 8.8° moving ON object (red) and moving OFF object (black, n = 7 flies). A′). Pairwise comparison of maximum ΔF/F of responses from each preparation (***p<0.001, paired t-test, n = 7 flies). A″) Average maximum responses (±S.E.M.) of LC11 glomerulus to a stationary 30°by 8.8°OFF and ON object placed within the hotspot of the receptive field (n = 6 flies). B) Mean GCaMP6m signal from the LC11 glomerulus in response to varying contrast objects. Grayscale of the filled area is used to indicate the intensity of the visual

background, whereas grayscale of the response line indicates intensity of the stimulus object (n = 9 flies). The most contrasting objects do not elicit the maximum responses from LC11. B′) Average of maximum responses (±S.E.M.) of the LC11 glomerulus to objects of varying contrast. Schematic on the x-axis shows the intensity of the background compared to each object. Weber contrast values are indicated numerically (see Supplemental Experimental Procedures, one-way ANOVA, n = 9 flies). C–F) LC11 glomerulus responses to parameterized direction (C, C′), vertical height (D, D′) horizontal width (E, E′), and two-object separation distance (F, F′). Time series responses shown in A–F, and color coded parameter values and maximum responses (±S.E.M) shown in C′–F′. C and C′) LC11 is omni-directional. An 8.8° square object was moved in 8 different directions in 45° steps as indicated by color-coded arrowheads (n = 7 flies, see single cell responses in Figure S3). D and D′) LC11 is vertically size tuned. A 30° wide object was moved on the same horizontal trajectory, with varied vertical heights: 2.2°, 4.4°, 8.8°, 18°, 35°, 73.2°, colors mapped to object size in B′ (n = 7 flies). Vertical gray line indicates average receptive field (RF) size (Figure 2). E and E′) LC11 is horizontally size tuned. An object of fixed height (8.8°) and varied width: 2.2°, 4.4°, 8.8°, 18°, 35°, 70°, 210°, was moved horizontally (n = 15 flies). The leading edge of each object appeared on the LED display at the same time. Vertical gray line indicates average estimated functional RF size (Figure 2). F and F′) LC11 is inhibited by a second object. Two 8.8° square objects moved on parallel trajectories. The distance between them was 0°, 2.2°, 4.4°, 8.8°, 18° and 32°, colors mapped to separation distance in C′ (n = 6 flies). Vertical gray line indicates average RF size (Figure 2). See also Figure S3.

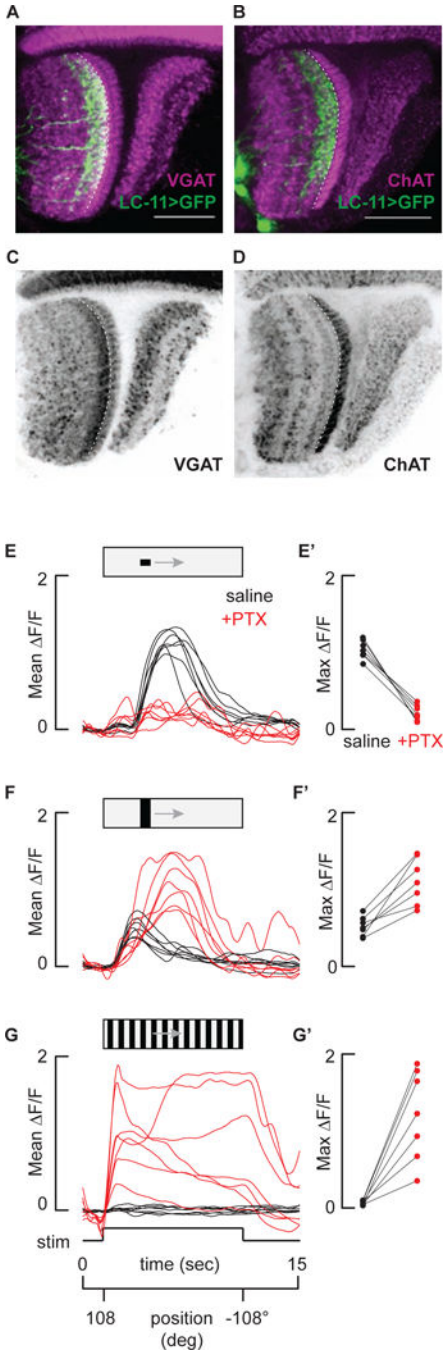

Figure 4. Both sensitivity and selectivity for objects by LC11 requires inhibition

A and B) LC11 dendritic layer is enriched with the vesicular GABA transporter (VGAT), and the adjacent presumably presynaptic layer is enriched with choline acetyltransferase (ChAT). Dorsal view of GFP labeled LC11 neurons (green) co-labeled with either anti-ChAT (A, magenta) or VGAT (B, magenta). Dashed line indicates the border between the first and second lobula strata. Scale bars 25 um. C and D) Layering of VGAT and ChAT are highlighted with the same labeling as in A and B, but without LC11 overlaid. Scale bars are 25 um. E – G) Inhibition sculpts object responses and inhibits bar and grating responses.

Time series glomerular LC11 responses from n = 7 flies in response to a 30°by 8.8° object (E), a 30° by 70° bar (F) and a wide-field grating (G) with (red) or without (black) 10 um picrotoxin. E′ – G′) Average maximum responses from each fly (E – G) with (red) or without (black) picrotoxin.